Information Process in Vestibular System

ALEXANDROV V. V.[1,3], ALEXANDROVA T. B.[2,3], VEGA R.[2] , CASTILLO QUIRÓZ G.[1],
ÁNGELES VÁZQUEZ A.[1], REYES ROMERO M.[1] and SOTO E.[2]

[1]Facultad de Ciencias Físico Matemáticas, Universidad Autónoma de Puebla, México,
[2] Instituto de Fisiología, Universidad Autónoma de Puebla, México, [3]Moscow State University.
Av. San Claudio y Río verde, Ciudad Universitaria, CP 72570, Puebla,
MÉXICO
vladimiralexandrov366@hotmail.com, esoto@siu.buap.mx, maribelrr@gmail.com

Abstract: A mathematical model of the output generation of the vestibular mechanoreceptor is presented. The model consider the series of events in the vestibular end organs that lead to the activation of the afferent neurons in the vestibular nerve and the generation of the afferent impulses. We have considered five compartments: mechano-electrical transduction, adaptation of transduction, hair cell ionic currents, synaptic transmission, and afferent neuron discharge. The numerical parameters of the model were obtained from experiments that were done in the inner ear of the rat. The results of the numerical analysis of the model showed that the mathematical modelling of the output from the vestibular mechanoreceptor may be used to construct an encoder system for artificial sensors (e.g.: vibrational gyroscope) contributing to the development of a reliable vestibular prosthesis prototype. This model can be used as the basis for the mathematical modelling of the vestibular sensors.

Key-Words: - Mechanical stimulus, hair cell, primary neuron, vestibular mechanoreceptor, afferent impulses

1 Introduction

In the vestibular end organs, the semicircular canals and the otolithic organs allow the perception of the influence of gravity and of the inertial forces produced by changes of the head position to provide information used to stabilize the gaze, the posture and contribute to generate a map of head direction in the space. Receptor hair cells of the vestibular system transform the energy of a mechanical stimulus into a voltage change and finally in a series of action potentials conducted to the central nervous system by the afferent neurons.

The series of processes leading to the sensory receptor activation and subsequent nervous system electrical discharges are summarized in the functional scheme of the vestibular mechanoreceptor shown in Fig.1. Displacement of the sensory hair bundle $x(t)$ activates the mechano-electrical transduction process which originates a transducer ionic current (I_{Tr}). This leads to a membrane potential change in the sensory cell (hair cell) that activates various voltage - dependent ionic channels in the hair cell (V_1). This series of events finally produces a voltage-dependent activation of calcium channels, and the subsequent activation of the neurotransmitter release machinery leading to synaptic activation of the afferent neurons in the vestibular nerve (I_{syn}). The primary afferents integrate the activity from various synaptic sources and accordingly generate a series of action potentials of a given frequency. These afferent impulses constitute the output from the vestibular

mechanoreceptor (Fig.1). Two levels of control that are acting in this system were considered in the model. An intrinsic one caused by the transducer adaptation mechanism [13] and an extrinsic one bring about by the efferent system innervation [12]. In this and previous works [1,2,3,4] we have developed a compartmental model of the vestibular mechanoreceptor. The model includes five compartments: mechano-electrical transduction, adaptation of transduction, hair cell ionic currents, synaptic transmission, and afferent neuron discharge. In relation to the control mechanisms, only the transducer adaptation mechanism has been considered, because the function of the efferent system originating from the central nervous system is still not well known.

2 Experimental methods

Experiments to study the hair cells were carried out using wild larval axolotls (*Ambystoma tigrinum*) or rats. Experiments for the study of ionic currents in vestibular primary afferent neurons were carried out using rats. All experiments were done as previously reported [7, 8]. Animal housing and experimental procedures were in accordance with the National Institutes of Health Guide for the Care and Use of Laboratory Animals and the Reglamento de la Ley General de Salud en Materia de Investigación para la Salud of the Secretaría de Salud of México.
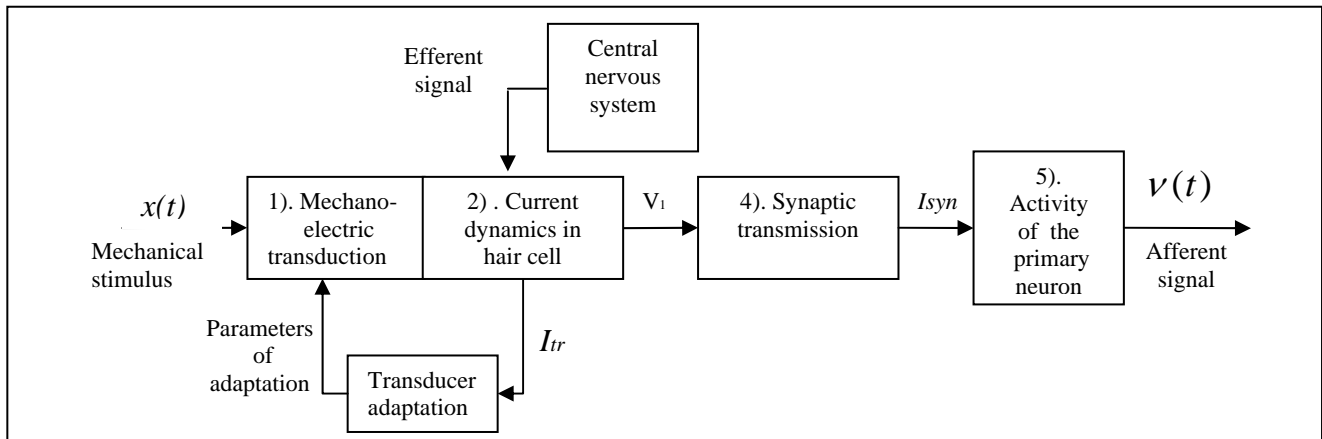
Fig.1. Scheme of the vestibular mechanoreceptor and the compartments considered in the model (1-5).

Hair cell and afferent neuron voltage clamp recordings. Vestibular end organs were dissected from the inner ear, and the hair cells was enzymatically dissociated. The cells were then transferred to the external Ringer solution (in mM): NaCl 111, KCl 2.5, $CaCl_2$ 1.8, $MgCl_2$ 1, HEPES 5, glucose 10, osmolarity 240 mOsm/Kg and the pH adjusted with NaOH to 7.4. Once the cells settled down, the recording chamber was continuously perfused with the normal external solution at a constant rate of 0.5 ml/min, using a peristaltic pump (LKB,Microperpex). The isolated cells were recorded with the use of the patch-clamp technique in the whole cell voltage-clamp configuration. Patch- clamp pipettes are fabricated from borosilicate (hard) glass capillary tubing of outside diameter 1.2 mm. The patch pipettes used for the whole-cell recording had resistances of 2-4 $M\Omega$ when filled with the intra-cellular solution.

Data were recorded with an Axopatch 200B amplifier (Axon Instruments) whose output led to a 12-bit digital-analog converter (Digidate 1200) controlled by the pClamp software (Axon Instruments). Data were low-pass filtered at 2 KHz and sampled at 100 µs intervals. Once the cell was touched with the electrode, the capacitive transients were nulled and time was allowed for the seal resistance (R_{seal}) between the cell and the electrode to grow above 1 $G\Omega$ (commonly, no negative pressure was needed for the seal resistance to grow, but in some experiments a slight negative pressure should de applied to establish the gigaohm seal). Once the gigaohm seal was established, the cell membrane was ruptured and the system went into the whole cell patch-clamp configuration; the access resistance, membrane resistance, membrane time constant, capacitance, and holding current were calculated on line by the pClamp software. However, a -10 mV pulse relative to

V_{hold} = -70 mV was registered in all the cells we studied. The current thus produced was used to measure (offline) the seal resistance, the capacitance and the membrane time constant (τ), from which the series resistance (R_s) of recording was calculated, since $\tau = R_s \times C$. Once the passive properties were recorded, the capacitive transient and series resistance were electronically compensated. The series resistance was compensated up to 80% with a 10 ms time lag.

The voltage-activated ionic currents were produced by using specifically designed voltage clamp protocols. The total ionic current was activated using a double-pulse voltage clamp protocol in which V_{hold} was -85 mV and a series of test pulses of duration 800 ms ranging from -130 to 50 mV (V_{test1}) in steps of 10 mV were followed by a 200 ms pulse to 20 mV (V_{tes2}). The first pulse series allowed measuring the activation parameters of the current and the inactivation time constant. The second pulse series allowed defining the steady-state inactivation of the total current.

For the current-clamp experiments, the cell membrane potential was set to – 70 mV by current injection. A series of current pulses ranging from -0.5 to 0.5 nA and with the duration of 800 ms were applied with intervals of 5 s.

3 Mathematical model
In sections 3.1 and 3.2 the basic model consisting of the: "Current dynamics in hair cells" and "Afferent neuron dynamics" are presented. In section 3.3 these two blocks are connected by the "Synaptic transmission" block. Also described are the input of the "Mechanoelectric transduction" and the "Transducer adaptation" to prolonged mechanical stimulus.

Alexandrov V. V, Alexandrova T. B, Vega R, Castillo Quiroz G,
Angeles Vazquez A, Reyes Romero M and Soto E

3.1 Current dynamics in hair cells

The model is based on the Hodgkin-Huxley equations. This is a simplified model, assuming that the dynamics of a hair cell may be described using a single total ionic current I_T [1], where I_T is the sum of the principal currents of the hair cells. The model is summarised in (1)

$$C_{m1}\frac{dV_1}{dt} = I_{com} - I_T - I_{L1},$$

$$I_T = g_T m^r (h_1 + h_2)(V_1 - E_T),$$

$$I_{L1} = g_L V_1,$$

$$\tau_m(V_1)\frac{dm}{dt} = m_{ST}(V_1) - m, \qquad (1)$$

$$\tau_{h1}(V_1)\frac{dh_1}{dt} = q_1 h_{ST}(V_1) - h_1,$$

$$\tau_{h2}(V_1)\frac{dh_2}{dt} = q_2 h_{ST}(V_1) - h_2,$$

Here I_T is the total current flowing through voltage-dependent ionic channels, E_T is the equilibrium potential for the total current (in the hair cells, this last variable is very close to the K^+ equilibrium potential, i.e., $E_T \approx E_K$). m is the parameter that specifies the current activation process, h is the parameter that specifies the current inactivation process; g_T is the maximal value of the conductance; I_{L1} is the leakage current; and I_{com} is, under natural conditions, the current flowing into a hair cell through the transduction channels situated in stereocilia ($I_{com} = -I_{Tr}$), or in the experiments, the command current. The inactivation parameter h has two constituents ($h = h_1 + h_2$) corresponding to the potassium channels with fast and slow inactivation time constants. Here q_1 and q_2 have their values between 0 and 1 and are the relative weights of the fast and slow inactivations, respectively. The voltage dependence of m, h_1 and h_2 are given by the functions m_{ST} and h_{ST}. These functions can be described as the first order Boltzmann functions. The activation and inactivation time constants, in the general case, are also functions of voltage (V_1). According to the results of our computations confirmed by the data from the literature, we found that the inactivation time constants τ_{h1} and τ_{h2} depend on the voltage (V_1) weakly. It is quite enough to approximate τ_{h1} and τ_{h2} by straight lines with small slope angles with the parameters k_{h1}, k_{h2}, b_{h1}, and b_{h2}. The functional parameters are shown in Table 1.

Name	Functional parameters
Steady-state activation	$m_{ST}(V_1) = m_{\min} + \dfrac{1 - m_{\min}}{1 + \exp\left(\dfrac{-(V_1 - V_{ac})}{S_{ac}}\right)}$
Activation Time constant	$\tau_m(V_1) = \tau_{\min} + \dfrac{\tau_{\max} - \tau_{\min}}{1 + \exp\left(\dfrac{V_1 - V_\tau}{S_\tau}\right)}$
Steady-state Inactivation	$h_{ST}(V_1) = h_{\min} + \dfrac{1 - h_{\min}}{1 + \exp\left(\dfrac{V_1 - V_h}{S_h}\right)}$
Fast inactivation Time constant	$\tau_{h1}(V_1) = k_{h1}V_1 + b_{h1}$
Slow inactivation Time constant	$\tau_{h2}(V_1) = k_{h2}V_1 + b_{h2}$

Table 1. Functional parameters of the model used in (1).

The numerical parameters entering into Table 1 were obtained from experimental voltage-clamp recordings of the isolated hair cells from the semicircular canal of the axolotl and the rat [5,6] (Table 2).

Parameter name	Semicircular canal from the axolotl	Semicircular canal from the rat
C_{m1}	$14.3 \pm 1.23\, pF$	$11.26 \pm 4.92\, pF$
g_L	$2.32 \pm 0.48\, nS$	$2.32 \pm 0.48\, nS$
g_T	$78.51 \pm 17\, nS$	$77.84 \pm 3\, nS$
E_T	$-87 \pm 15\, mV$	$-79 \pm 7\, mV$
I_{com}	$0 \pm 300\, pA$	$0 \pm 300\, pA$
$\tau_{\max}$	$11.41 \pm 2.56\, ms$	$77.58 \pm 4.23\, ms$
$\tau_{\min}$	$0.38 \pm 0.03\, ms$	$6.55 \pm 0.31\, ms$
V_τ	$-68.47 \pm 7.35\, mV$	$-5223 \pm 6.89\, mV$
S_τ	$14.95 \pm 2.72\, mV$	$15.68 \pm 3.15\, mV$
V_{ac}	$-47.6 \pm 7.3\, mV$	$-25.36 \pm 5.09\, mV$
S_{ac}	$15.2 \pm 2.5\, mV$	$15.06 \pm 2.47\, mV$
m_{mim}	0.25 ± 0.13	0.37 ± 0.21
k_{h1}	$-0.04 \pm 0.05\, \dfrac{ms}{mV}$	$0.82 \pm 0.25\, \dfrac{ms}{mV}$

Alexandrov V. V, Alexandrova T. B, Vega R, Castillo Quiroz G, Angeles Vazquez A, Reyes Romero M and Soto E

k_{h2}	$0.14 \pm 0.28 \dfrac{ms}{mV}$	$1.26 \pm 0.97 \dfrac{ms}{mV}$
b_{h1}	$45.08 \pm 15.84\, ms$	$55.86 \pm 14.28\, ms$
b_{h2}	$129.49 \pm 22.25\, ms$	$282.38 \pm 57.49\, ms$
V_h	$-65.23 \pm 2.42\, mV$	$-9.82 \pm 1.98\, mV$
S_h	$7.26 \pm 1.28\, mV$	$21.96 \pm 2.80\, mV$
$h_{\min}$	0.38 ± 0.06	0.73 ± 0.14
r	3	3

Table 2. Hair cells numerical parameters of the semicircular canal from the axolotl and from the rat.
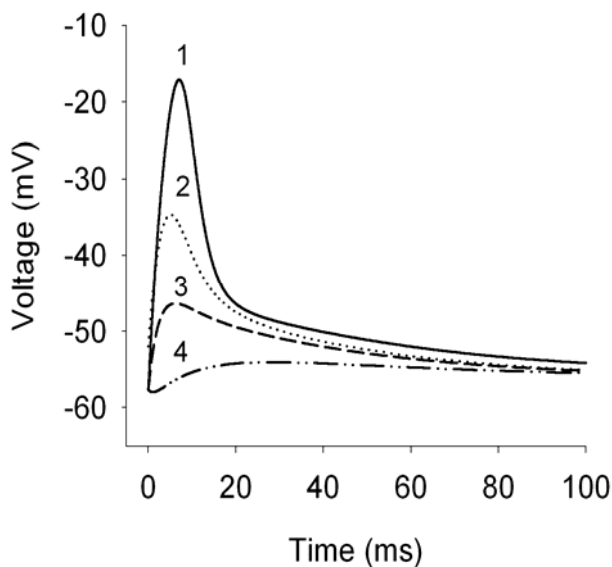

Fig. 2. Voltage response trajectories obtained for I_{com} = 0. These traces were obtained for different initial conditions taken for system (1):

(1) V_0 = -57.67 mV, m = 0.0041, h_1 = 0.9, h_2 = 0.1;

(2) V_0 = -52 mV, m = 0.240, h_1 = 0.8, h_2 = 0.2;

(3) V_0 = -57.67 mV, m = 0.340, h_1 = 0.8, h_2 = 0.2;

(4) V_0 = -57.67 mV, m = 0.440, h_1 = 0.8, h_2 = 0.2.

The numerical data taken from Table 1 and 2 for system (1) correspond to mean values of the parameters for the semicircular canal hair cells from the rat.

In Fig. 2 are the voltage responses trajectories from system (1) obtained for I=0. Using the values shown in table 1 and 2, the model predicted a resting potential of -57 mV as well as a damped potential oscillation in response to depolarizing current pulses and a passive response to hyperpolarizing stimulus. The voltage response to current injection in hair cells is in consequence characterized by a quasilinear voltage change to hyperpolarizing currents and a

nonlinear response to depolarizing currents, thereby indicating that the input resistance decreases with depolarization. (Fig. 3). The dynamics of the hair cell membrane potential, obtained with the use of the mathematical model shown in (1), qualitatively coincides with the results of the physiological experiments.
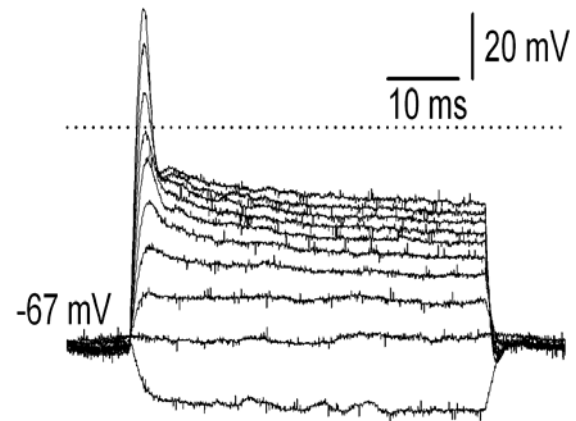

Fig. 3. Traces showing a typical voltage response of a hair cell obtained from the rat's semicircular canals subjected to current pulse injection (from -0.1 to 0.5 nA). The dotted line shows the zero voltage

The total ionic current was studied using different cells from the semicircular canals from the axolotl and rat. The functions $m_{ST}(V)$, $h_{ST}(V)$, $\tau_m(V)$, $\tau_{h1}(V)$, and $\tau_{h2}(V)$ are illustrated in graphic form (see Fig.4 and Fig.5). The numerical data taken for this graphs correspond to mean values of the parameters.

It is worth noting that, due to a complex nature and, in some cases, nonlinear behavior of the total ionic current in the hair cells, simple models cannot adjust some of the experimental recordings, indicating that more detailed models should be developed. Since, in addition, the complex nonlinear phenomena were found in our experiments, more detailed models should be developed.

To determine the current inactivation time constant, an exponential function was adjusted to the current. The filter properties of the semicircular canal hair cells from the axolotl and the rat are different. A single exponential did not produce a correct adjustment to the inactivation time course; therefore, we decided to use two exponential functions to fit the inactivation of the current. Both τ_{h1} and τ_{h2} did not display a very clear voltage dependence (Figure 5,B and C).

Alexandrov V. V, Alexandrova T. B, Vega R, Castillo Quiroz G,
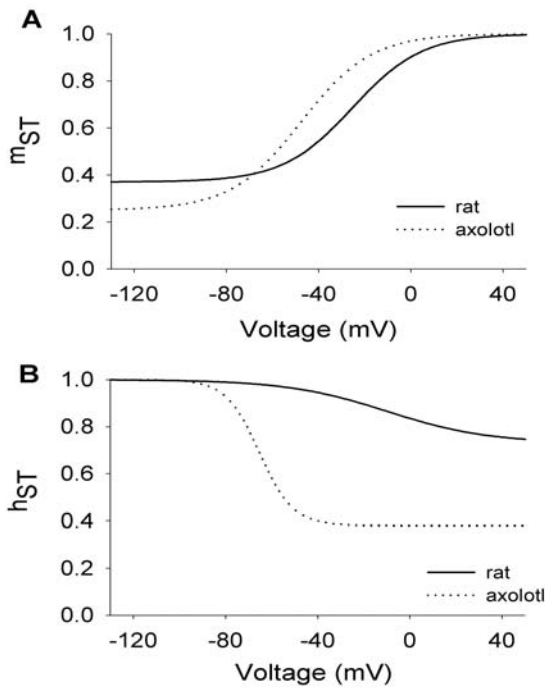Angeles Vazquez A, Reyes Romero M and Soto E

Fig.4. Comparison of the properties of the total current in the semicircular canal hair cells from the axolotl and rat. A and B: show the curves of the activation (m) and inactivation (h) of the current as functions of voltage respectively.
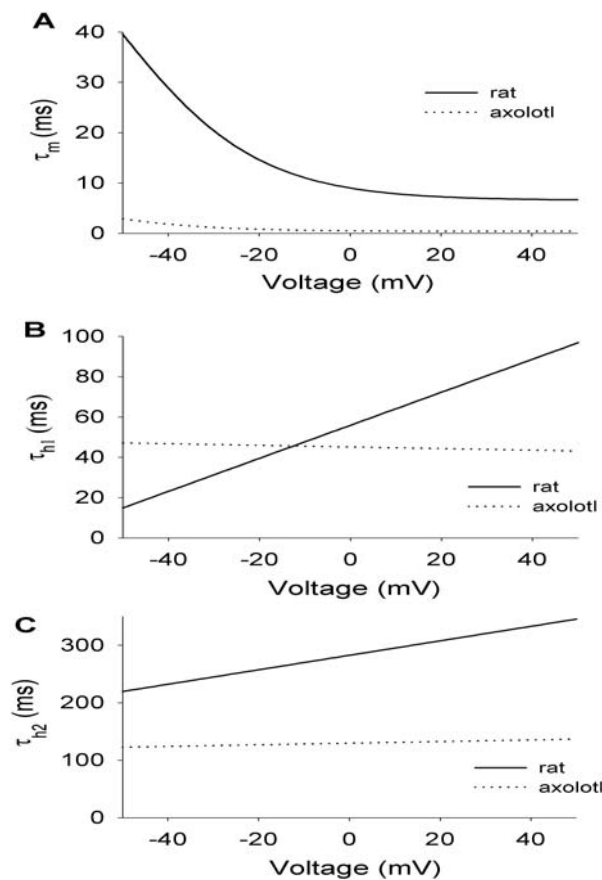
Fig.5. Comparison of the properties of the total current in the semicircular canal hair cells from the axolotl and rat. A: plot of τ_m versus voltage. τ_m depends exponentially on the voltage. These values were approximated by a Boltzmann function. B and C: plots of τ_{h1} and τ_{h2} as functions of voltage were fitted with straight lines, thus indicating that the inactivation time constant had not a clear voltage dependence.

The mathematical model (1) and the correctness of parameter values can be validated by the comparison of model results with experimental data from the axolotl, using the current clamp protocol for certain cell types. We have used a computer program to obtain the current clamp protocol for the influences I_{com} = -300 pA, -200 pA, -100 pA, 0 pA, 100 pA, 200 pA, and 300 pA. The general properties of voltage responses to the pulsed current in type II hair cells are: a passive response to a hyperpolarizing stimulus and a damped oscillatory response to a depolarizing stimulus.

In Fig.6 compares the current clamp experimental results with our model results. The mathematical model satisfactorily reproduces the voltage response of hair cells to the current injection.
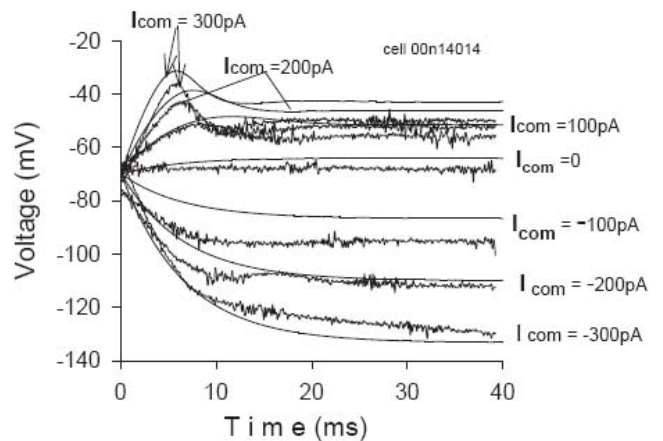

Fig. 6. Comparison of the experimentally measured response to current pulses from -300 to 300 pA (in steps of 100 pA) in a semicircular canal hair cell (00N14014) from the axolotl with the model voltage response trajectories. The thin (without noise) curves correspond to the model results. Parameter values in the model were chosen to produce accurate fits of the current response in the voltage clamp for the cell being studied. The model parameters were: C_{m1} = 15 pF, g_L = 1.5 nS, g_T = 79 nS, E_T = -105 mV, h_{min} = 0.115, V_h = -53.1 mV, S_h = 12.1 mV, r = 3, m_{min} = 0.164, V_{ac} = -29 mV, S_{ac} = 9.09 mV, τ_m = 0.396 +

93.77/(1+ $exp((V_1 + 86.34)/14.24))$ ms, τ_{h1} = -0.233 V_1 + 1.54 ms, τ_{h2} = -0.778 V_1 +213.9 ms. The model predicted a resting potential of -67 mV as well as a damped potential oscillation in response to depolarizing current pulses followed by a slowly developing depolarization and a passive response to hyperpolarizing stimulus.

In Fig.7, are the voltage response trajectories obtained for different I_{com}. The dynamics of the hair cell membrane potential, obtained with the use of the mathematical model shown in (1), qualitatively coincides with the results of the physiological experiments from the rat. Comparing the figures 6 and 7 it is found that voltage response trajectories obtained for different I_{com} were similar.
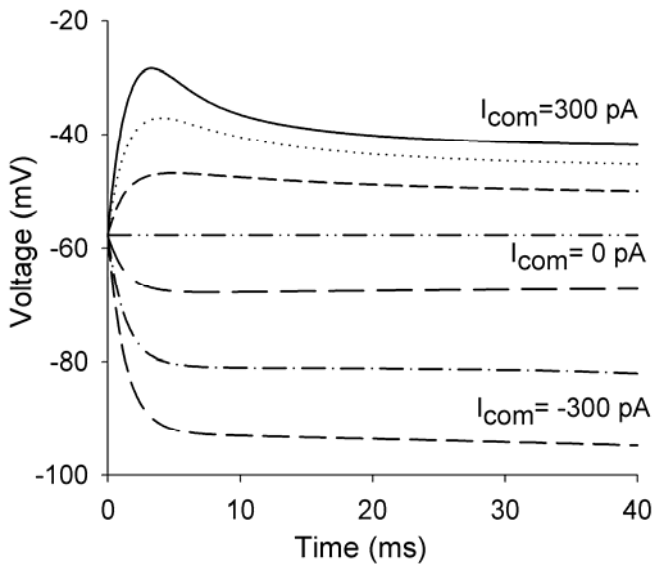

Fig. 7. Voltage response trajectories obtained for different I_{com}. (from -300pA to 300 pA). These traces were obtained for an alone one initial condition take for system (1) with the numerical data taken from Table 1 and 2 of the semicircular canal hair cells from the rat.

3.2 Afferent neuron dynamics

To model the activity of the primary afferent bipolar neuron, a Hodgkin-Huxley-type model was also used. The parameters were calculated using experimental results obtained from cultured vestibular afferent neurons of the rat [7,8]. The use of rat parameters in this model is the first modification with respect to the original Hodgkin-Huxley model. Two additional modifications were about the time constants: an inactivation parameter for outward current "h_K" other is a modification in the mathematical model original of Hodgkin-Huxley $h + n$ =0.8, here we have next

modification $h + n=C(V_2)$, $C(V_2)$ is a experimental results. The right part of this equality has a constant value for each $V_2 \in$ [-100 mV, 100 mV]. In addition, our model have a complex description for potassium current $I_K = g_K^{max} n^4 h_K (V_2 - V_K)$. Based on these modifications and assuming that $\tau_m = 0$ and τ_{hk} = constant an intersection of two isoclines as an unstable point of repose was found.

The V_2 isocline is defined by $\dfrac{dV_2}{dt} = 0$ and has a cubic shape, while the n isocline is defined by $\dfrac{dn}{dt} = 0$ and is monotonically increasing. There is a single intersection and thus a single steady state (Fig.8). Therefore, a limit cycle and the correspondent auto-oscillations were also found.
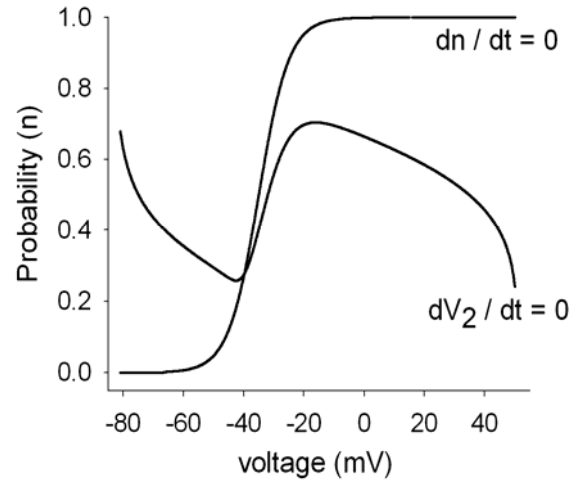

Fig. 8. Isoclines of the simplified and of the modified Hodgkin-Huxley model.

The modified and simplified Hodgkin-Huxley model (see above) for the action potential generation takes the form as shown in [4].

$$C_{m2} \frac{dV_2}{dt} = I_{com} - I_{Na} - I_K - I_{L2},$$

$$I_{Na} = g_{Na}^{max} (m_\infty(V_2))^3 (C(V_2) - n)(V_2 - V_{Na}),$$

$$I_K = g_K^{max} n^4 h_K (V_2 - V_K),$$

$$I_{L2} = g_L^{max} (V_2 - V_L),$$

$$\tau_n(V_2) \frac{dn}{dt} = n_\infty(V_2) - n, \qquad (2)$$

$$\tau_{h_K}(V_2) \frac{dh_K}{dt} = h_{K\infty}(V_2) - h_K.$$

Here the subscripts *K*; *Na*; and *L2* correspond to potassium, sodium, and leakage channels, respectively.

The coefficients g_{Na}^{max}, g_K^{max}, g_L^{max} belong to confidence intervals in accordance with the experimental results. Table 3 presents coefficients m_∞, $h_{Na\infty}$, n_∞, $h_{K\infty}$, τ_{hNa}, τ_n, τ_{h_K} and C in an additional approach which can be expressed by functions depending on the potential V_2. Table 4 presents the values which correspond to the greatest interval between two points (I_1, I_2) of the bifurcation of Hopf [9]. These points indicate the appearance and disappearance of the auto-oscillations.

Name	Functional parameters
Activation stable state g_{Na}	$m_\infty(V_2) = \dfrac{1}{1+\exp\left(\dfrac{-(V_2+33.8)}{5.2}\right)}$
Inactivation stable state g_{Na}	$h_{Na_\infty}(V_2) = \dfrac{1}{1+\exp\left(\dfrac{V_2+60.5}{9.9}\right)}$
Inactivation time constant g_{Na}	$\tau_{hNa}(V_2) = \dfrac{1}{0.01+\exp\left(\dfrac{79+V_2}{-15}\right)+\exp\left(\dfrac{30+V_2}{5}\right)}+0.5$
Activation stable state g_K	$n_\infty(V_2) = \dfrac{1}{1+\exp\left(\dfrac{-(V_2+35)}{5}\right)}$
Inactivation stable state g_K	$h_{K\infty}(V_2) = \dfrac{0.96408-0.7329}{1+\exp\left(\dfrac{V_2+33.87968}{10.24986}\right)}+0.7329$
Activation time constant g_K	$\tau_n(V_2) = \dfrac{68}{\exp\left(\dfrac{25+V_2}{-15}\right)+\exp\left(\dfrac{30+V_2}{20}\right)}$
Inactivation time constant g_K	$\tau_{h_K}(V_2) = \dfrac{1250}{\exp\left(\dfrac{15+V_2}{-15}\right)+\exp\left(\dfrac{25+V_2}{10}\right)}+500$

$$C(V_2) = n_\infty(V_2) + h_{Na_\infty}(V_2)$$

Table 3. Functional parameters of the model for vestibular afferent neurons (2).

Constants	Units	Chosen Value
C_{m2}	$\mu F/cm^2$	1
V_{Na}	mV	52
V_K	mV	-84
V_L	mV	-63
g_{Na}^{max}	mS/cm^2	2.3
g_K^{max}	mS/cm^2	2.4
g_L^{max}	mS/cm^2	0.03
I_{com}	$\mu A/cm^2$	1 to 150

Table 4. Numerical parameters of model (2).

The amplitude of the auto-oscillations depends on the value of I_{com} (where $I_{com}= -I_{syn}$).

The limit cycles thus obtained are shown in Fig. 9 and 10. Those correspond to two points in the vicinity of the points of bifurcation of Hopf. The first point of bifurcation $I_1 = 0.6$ $\mu A/cm^2$, the second point of bifurcation of Hopf $I_2 = 165.3$ $\mu A/cm^2$.
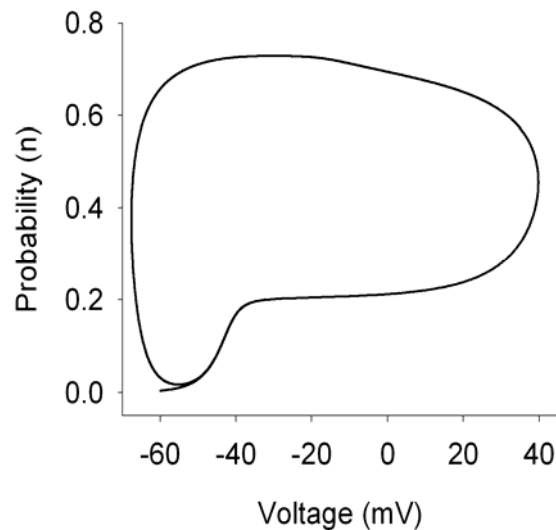

Fig.9. A cycle limit obtained using the values in the table 3 and $I_{com} = 0.63$ $\mu A/cm^2$.

This cycle limit occurs when the flow $I_{com} = 0.63$ $\mu A/cm^2$, consists of a range of approximately 120 mV, due to the dynamics of the ions (Na^+ and K^+).

If the value of the constant synaptic current belongs to the interval between the points of bifurcation, then the point of intersection of the isoclinal lines is always located on the middle part of the isoclinal line $dV_2/dt = 0$ and is unstable (Fig. 8). This leads to the formation of auto-oscillations with changing

frequencies. A change of the frequency is the information carrier. Thus, a change in the membrane potential of the hair cell, which is been primary information about the stimulus, is represented in the convenient form for the transfer to the central nervous system.
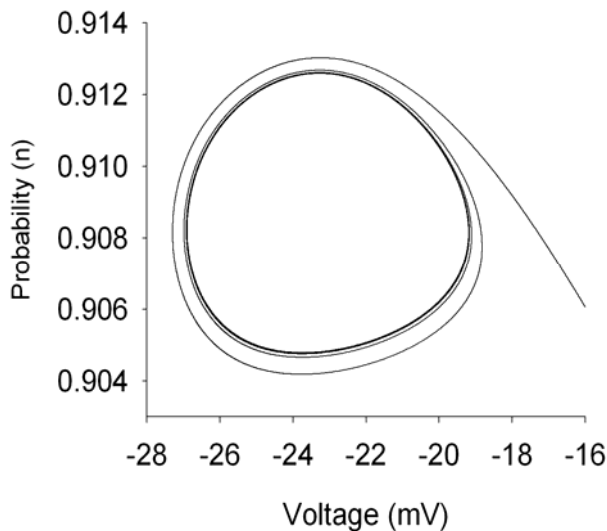

Fig.10. A cycle limit obtained using the values in Table 3 and $I_{com} = 98\ \mu A/cm^2$.

3.3 Synaptic transmission, mechano- electrical transduction and transducer adaptation

Data from experimental studies of synaptic transmission in the bullfrog inner ear [10] were used for the association of the blocks which describe the dynamics of ionic currents in the hair cell and in the primary afferent neuron (Fig. 1). The curve shown in Figure 11 shows the relationship between the voltage in the hair cell (V_1 in model 1) and the synaptic current in the afferent neuron (I_{syn} equivalent to I_{com}). The maximum synaptic current was hypothesized to be equivalent to $40\ \mu A/cm^2$.

This result was obtained using the experiments in the hair cells of amphibians. For this reason we made a comparative analysis of the difference between the stationary values of the membrane potential and the total current of the hair cell of amphibians (axolotls) and the values corresponding to mammalians (rats). The results of the comparison with the intervals of confidence for g_T and g_L are presented in the Fig. 12 with I_{com}=0. The existence of the insignificant difference between these values provides us the special arguments for the use of the

curve of the synaptic current with dependency of the potential of the membrane of the hair cell that is displayed in Fig.11.

Let us add, to the chain of three blocks just described, an input block for the mechano-electrical transduction mechanism [1], and the mechanism of the hair cell transducer adaptation to the prolonged mechanical stimuli. The mathematical model of these two mechanisms is represented in the form of equation (3).
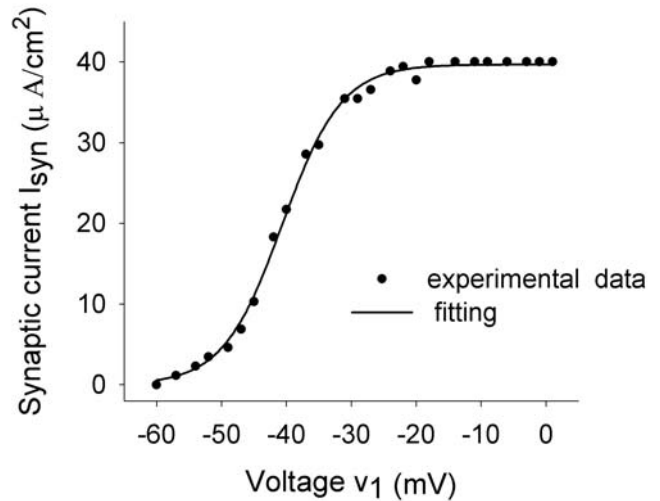

Fig. 11. Relationship between hair cell voltage and synaptic current in the afferent neuron. Data calculated from the experimental results of the bullfrog sacculus [10].
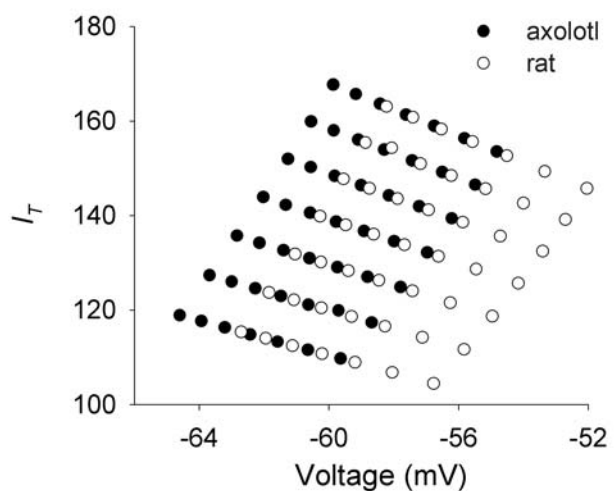

Fig.12. Comparative analysis of the stationary values of the total ionic current I_T and the membrane potential of the hair cells of amphibians and mammalians. These results are the comparison with the intervals of confidence for g_T and g_L.

The information for axolotls is indicated by black circles. The information for rats is indicated by white circles.

The adaptation mechanism is given by [4]:

$$\tau_{ad}\,\dot{s} + s = k(I_{Tr} - I_{Tro});\qquad(3)$$

$$I_{Tr} = g_{Tr}(x,s)(V_1 - E_{Tr});$$

$$g_{Tr} = \overline{g}_{Tr}\,p(x,s);$$

$$p(x,s) = \frac{1}{1 + Exp\left(-\dfrac{x + s - x_0}{s_1}\right)};$$

$$\tau_{ad} = 100\ ms;$$

$$k = 0.03;$$

$$I_{Tr0} = -14.4\ pA;$$

$$E_{Tr} = 0;$$

$$\overline{g}_{Tr} = 1.4\ nS;$$

$$x_0 = 0.3\ \mu m;$$

$$s_1 = 0.2\ \mu m.$$

Where s is the adaptation parameter; τ_{ad} is a time constant; k is a gain constant; I_{Tr} is the transduction current; I_{Tr0} is the transduction current in stationary state; $p(x,s)$ is the probability of the opening of the canal; x is the displacement of a hair bundle.

Using this system, a mathematical model of the vestibular mechanoreceptor information output was obtained. It consists of equations (1), (2), (3), Tables 1, 2, 3 and 4 and the graph in Fig.11.

4 Numerical results

After the association of all blocks of the model and the analysis of the dynamics of ion currents in the hair cell and in primary afferent neuron, the numerical parameters were selected on the basis of physiological experiments (Tables 1, 2, 3 and 4). The results of the calculations are shown in Fig.13. The mechanical stimulus is absent during the first 100 *ms* (stationary situation of rest); in the course of the following 200 *ms* the hair bundle is displaced on 1 *μm*. Formation of the primary information of membrane potential V_1 of hair cell as a result of the mechanism of adaptation. Finally we have secondary information in form of afferent impulses of primary neuron with different frequency (from 20 Hz to 40 Hz). The stimulus induced the afferent

neuron discharge to change from 20 Hz - in the absence of mechanical stimulus; to 40 Hz - with the beginning of mechanical stimulus.
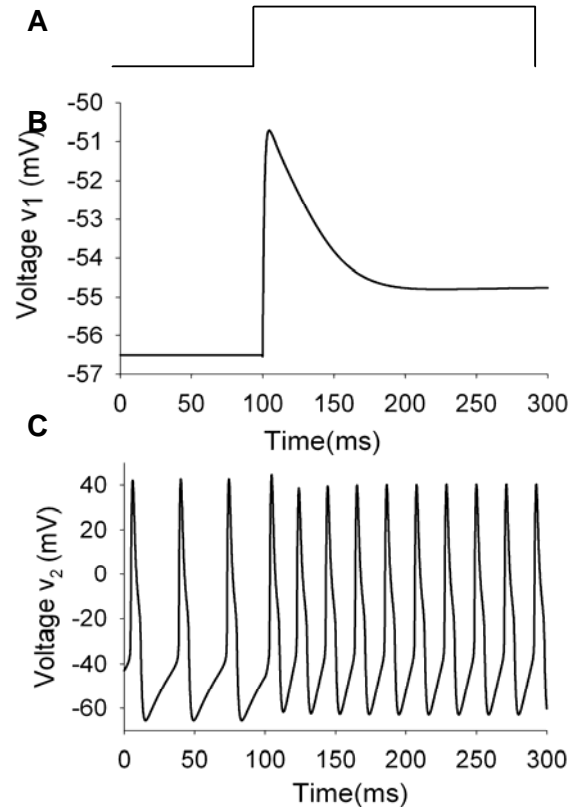

Fig. 13. The process of the information output from the vestibular mechanoreceptor. In A, the mechanical stimulus displaces a hair cell bundle. The stimulus is absent during the first 100 *ms* (stationary situation of rest); in the course of the following 200 *ms* the hair bundle is displaced on 1 *μm*. In B, the voltage response of the hair cell reflects the activation of the transducer adaptation mechanism. In C, the output of the model in the form of the action potentials in the primary afferent neuron is presented.

In Fig.14 shows the reponse of hair cell and afferent neuron (information process) in second vestibular mechanoreceptor. First and second mechanoreceptors has the same axis of sensibility but opposite polarity directions. The stimulus induced the afferent neuron discharge to change from 20 Hz - in the absence of mechanical stimulus; to 15 Hz - with the beginning of mechanical stimulus.

Alexandrov V. V, Alexandrova T. B, Vega R, Castillo Quiroz G, Angeles Vazquez A, Reyes Romero M and Soto E

Fig. 14. The process of the information output from the vestibular mechanoreceptor. The stimulus is absent during the first 100 *ms*; in the course of the following 200 *ms* the hair bundle is displaced on 1 μm (similar to Figure 13-A). In A, the voltage response of the hair cell reflects the activation of the transducer adaptation mechanism. In B, the output of the model in the form of the action potentials in the primary afferent neuron is presented, the stimulus induced the afferent neuron discharge to change from 20 Hz - in the absence of mechanical stimulus; to 15 Hz - with the beginning of mechanical stimulus.
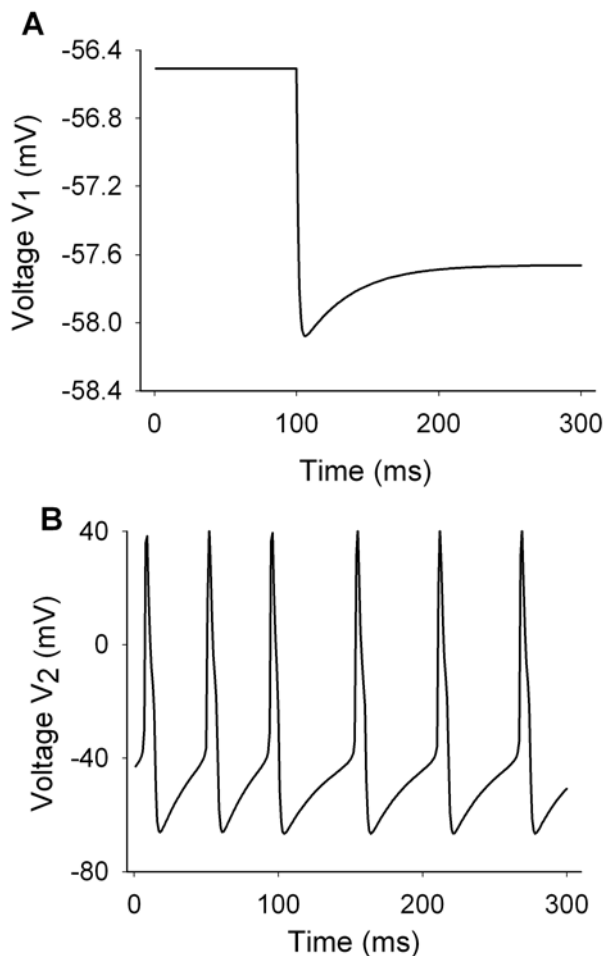
From Fig. 13 and 14, there can then be observed an information process in two vestibular mechanoreceptors with the same axis of sensibility, but with opposite positive directions. Can be noted changes in secondary information (20 - 40 Hz o 20 - 15 Hz) when the potential V_1 take values to the right or the left of the stable point (-56.5 *mV*) (Figure 11).

5 Conclusion

The numerical results indicate that the mathematical model of information processing in the vestibular mechanoreceptor resembles the activity of the natural sensor as studied experimentally.

In the development of vestibular prosthetic devices, a sigmoidal transfer function derived from the recordings in the monkey inner ear [11] has been used to convert the analog output of the device to a pulse train useful to stimulate the afferent nerve. We propose that using more realistic models based on physiological knowledge and using parameters from animal experiments will endow prosthetic devices with greater coding capabilities than those of devices using the simpler transfer functions.

Our results demonstrate that the development of an integrated mathematical model of the function of vestibular end organs is feasible and that it will resemble vestibular system coding capabilities.

It is concluded that the proposed mathematical model may be used to construct an encoder system for artificial sensors (eg: microaccelerometer and vibrational gyroscope) contributing to the development of a reliable vestibular prosthesis prototype.

References:
[1] Alexandrov V. V., Almanza A., Kulikovskaya N. V., Vega R., Alexandrova T. B., Shulenina N. E., Limón A. and Soto E. A Mathematical Model of the Total Current Dynamics in Hair Cells, In: *Mathematical Modeling of Complex Information Processing Systems,* pp 26-41, Moscow State University, 2001.

[2] Alexandrov V.V., Alexandrova T. B., Astakhova T. G., Kulikovskaya N.V., Kurilov V. I., Migunov S. S., Shulenina N.E., Soto E., Vega R. A mathematical model of the response of semicircular canal and otolith to head rotation under gravity. *J Gravitational Physiology*, 11(2) (2004) 25-26.

[3] Alexandrov V.V., Alexandrova T. B., Migunov S. S. The mathematical model of the gravity-inertial mechanoreceptor. *Moscow University Mechanics Bulletin*, No. 2, (2006) 59-64 .

[4] Alexandrov V.V., Mikhaleva E. Yu., Soto E., García Tamayo R. Modification of Hodgkin-Huxley mathematical model for the primary neuron of vestibular apparatus. *Moscow University Mechanics Bulletin,* No. 5 (2006) 65-68.

[5] Almanza A.., Vega R., and Soto E. Calcium current in type I hair cells isolated from the semicircular canal crista ampullaris of the rat. *Brain Research* 994 (2003) 175-180.

[6] Almanza A., Vega R., Naverrete F., and Soto E. Nitric oxide modulation of L type Ca^{2+} current in sensory hair cells. *J Neurophysiology,* 97 (2007) 1188-1195.

[7] Soto E., Limón A., Ortega A., and Vega R. Características morfológicas y electrofisiológicas de las neuronas del ganglio vestibular en cultivo. *Gaceta Médica de México,* 138 (2002) 1-14.

[8] Limón A., Pérez C., Vega R., and Soto E. IK,Ca current density is correlated with soma size in vestibular primary afferent neurons. *J Neurophysiology,* 94 (2005) 3751-3761.

[9] Troy W.C. The Bifurcation of periodic solutions in the Hodgkin-Huxley equations. *Quarterly of Applied Mathematics*, 36 (1978) 73-83.

[10] Keen E.C. and Hudspeth A.J. Transfer characteristic of the hair cell's afferent synapse. *Proc. Natl. Acad. Sci. USA,* 103 (2006) 5437-5542.

[11] Fernández G. and Goldberg J. Physiology of peripheral neurons innervating otolith organs of the squirrel monkey. II. Directional selectivity and force-response relations. *J Neurophysiology,* 29 (1976) 985-995.

[12] Goldberg J. and Fernández G. Efferent vestibular system in the squirrel monkey: anatomical localization and influence on afferent activity. *J. Neurophysiology,* 43 (1980) 986-1025

[13] Holt J. R. and Corey D. P. Two mechanisms for transducer adaptation in vertebrate hair cells. *Proc. Natl Acad. Sci. (USA)* 97 (2000) 11730-11735.